Absolute partial cross sections for electron-impact ionization of CO_2 from threshold to 1000 eV

H. C. Straub, B. G. Lindsay, K. A. Smith, and R. F. Stebbings
Department of Physics, Department of Space Physics and Astronomy, and Rice Quantum Institute, Rice University, Post Office Box 1892, Houston, Texas 77251

(Received 8 April 1996; accepted 3 June 1996)

Absolute partial cross sections for the production of CO_2^+, CO^+, CO_2^{2+}, O^+, C^+, O^{2+}, and C^{2+} from electron-impact ionization of CO_2 are reported for electron energies from threshold to 1000 eV. The product ions are mass analyzed using a time-of-flight mass spectrometer and detected with a position-sensitive detector whose output provides clear evidence that all product ions are completely collected. The overall uncertainty in the absolute cross section values is $\pm 3.5\%$ for singly charged parent ions and is slightly greater for fragment and doubly charged ions. For the fragment ion cross sections, all but one of the previous measurements are observed to be significantly lower than the present results. © *1996 American Institute of Physics.* [S0021-9606(96)01434-1]

I. INTRODUCTION

Ionization of atoms and molecules by electron impact is of fundamental importance in atmospheric science, plasma processes, and mass spectrometry. Comprehensive reviews[1–4] reveal large discrepancies in both the magnitude and energy dependences of cross sections reported by different groups. In many instances, limitations of the available instruments compromised the accuracy of the earlier measurements. The focus of this particular paper is electron-impact ionization of CO_2 for which there remain large uncertainties in the partial cross sections even though CO_2 is important in many environments.

Absolute total cross sections for CO_2 have been measured by Rapp and Englander-Golden[5] and by Asundi, Craggs, and Kurepa[6] using the parallel plate system pioneered by Tate and Smith.[7] Partial cross sections for CO_2 have been previously measured using various types of mass spectrometry by Freund, Wetzel, and Shul;[8] Orient and Srivastava;[9] Mark and Hílle;[10] Crowe and McConkey;[11] Adamczyk, Boerboom, and Lukasiewicz;[12] and Krishnakumar.[13] Of all the previous partial cross section measurements, however, only the work of Freund, Wetzel, and Shul[8] is absolute. All other partial cross section measurements were normalized using an absolute cross section determined by other researchers. Rapp, Englander-Golden, and Briglia,[14] who measured the cross section for production of ions with more than 0.25 eV of initial kinetic energy, were the first to study dissociative ionization of CO_2. Orient and Srivastava;[9] Crowe and McConkey;[11] and Adamczyk, Boerboom, and Lukasiewicz[12] measured partial cross sections for individual ions produced by dissociative ionization. Accurate determination of these cross sections is the most problematic due to the difficulties in assuring complete collection of all energetic fragment ions.

This paper reports absolute partial cross sections for electron-impact ionization of CO_2 using an apparatus and technique that allows the individual cross sections to be determined absolutely through direct measurement of all the quantities needed for their evaluation. The results are obtained using a time-of-flight mass spectrometer in which the mass analyzed ions are detected with a position-sensitive detector whose output demonstrates that all product ions, regardless of their initial kinetic energy, are completely collected. The measured processes are the production of CO_2^+, CO^+, CO_2^{2+}, O^+, C^+, O^{2+}, and C^{2+} for electron energies from threshold to 1000 eV.

II. APPARATUS AND EXPERIMENTAL METHOD

The apparatus shown in Fig. 1 is a time-of-flight mass spectrometer and has been described in detail previously.[15] Briefly, during a cross-section measurement the entire vacuum chamber is filled with carbon dioxide at a pressure of approximately 3×10^{-6} Torr. At a repetition rate of 2.5 kHz, 20 ns long pulses of approximately 2500 electrons are directed through an interaction region, located between two plates maintained at ground potential, and are collected in a Faraday cup. Approximately 200 ns after each electron pulse, a 480 V/cm electric field is applied across the interaction region to drive any positive ions formed by electron impact toward the bottom plate. This electric field is generated by applying a 3 kV pulse with a 55 ns rise time to the top plate. Some ions pass through a grid-covered aperture, of length 1.91 cm in the direction parallel to the electron beam, in the bottom plate. These ions are then accelerated to an energy of 5.4 keV for singly charged ions and subsequently impact a position-sensitive detector (PSD) that records both their arrival times and positions. The ion arrival times are used to identify their mass-to-charge ratios and the ion arrival positions serve to demonstrate complete collection of all product ions.

Under conditions in which very few of the incident electrons produce an ion, the partial cross section $\sigma(X)$ for production of ion species X is given by

$$\sigma(X)=\frac{N_i(X)}{N_e n l}, \tag{1}$$

where $N_i(X)$ is the number of X ions produced by a number N_e of electrons passing a distance l through a uniform gas

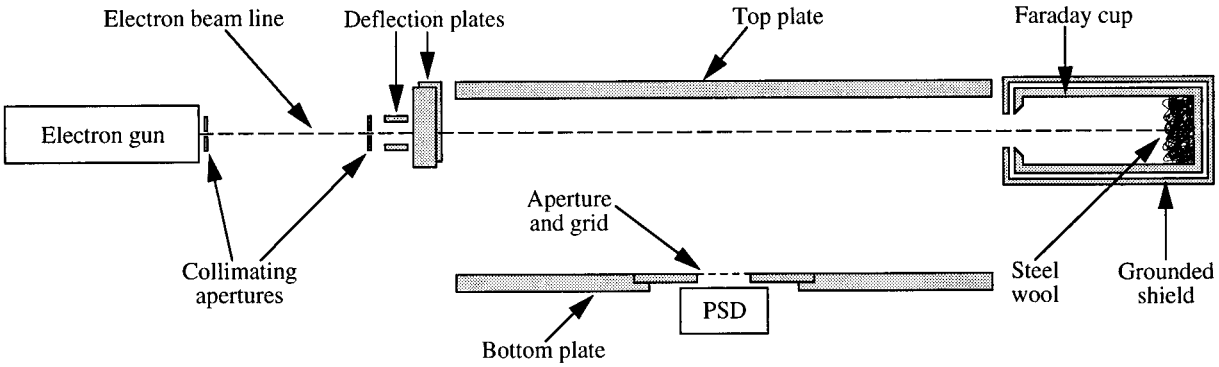

FIG. 1. Schematic diagram of the apparatus.

target of number density n. Determination of an absolute cross section requires measurement of all four quantities on the right-hand side of Eq. (1) and has been previously[15] described in detail except for the collection of energetic fragment ions from dissociative ionization. Briefly, the number of electrons N_e is determined by collecting the electron beam in a Faraday cup and measuring the current with an electrometer operating in the charge collection mode. Measurement of $N_i(X)$ is accomplished by recording the time-of-flight spectrum and counting the number ions in an appropriate portion of the spectrum. The effective path length l from which detected ions originate is accurately given by the 1.91 cm length of the aperture directly in front of the PSD. The target number density n is obtained from measurements of the target gas pressure using a capacitance diaphragm gauge.

Three minor changes were made to the previously described apparatus.[15] First, field shims at the edges of the interaction region were removed since they had no significant effect on the uniformity of the extraction field at the center of the interaction region. Second, a new high-voltage pulse generator, with a higher peak voltage and faster rise time, allowed easier collection of energetic fragments and increased the impact energy of ions on the PSD to 5.4 keV for singly charged ions. Third, the PSD, which comprises a pair of 25 mm diameter microchannel plate electron multipliers located in front of a resistive-encoded anode,[16] had a new set of microchannel plates installed. The detection efficiency for the combination of grid and PSD was determined to be $(37.8\pm0.2)\%$ by repetitively directing an ion beam of appropriate species and energy alternately onto the PSD and into a second Faraday cup (not shown in Fig. 1). The detection efficiency for the new set of microchannel plates was also found to be independent of the mass-to-charge ratio of the ions as was the case for the previous set of microchannel plates.[15] The 37.8% detection efficiency for the combination of grid and PSD results from a PSD detection efficiency of 58% and a grid transparency of 65%.

A typical time-of-flight spectrum for CO_2 is shown in Fig. 2, which demonstrates that the mass resolution is sufficient to separate the various product ions. The small contributions to the spectrum due to residual background gas are determined by removing the target gas from the vacuum chamber and again recording the time-of-flight spectrum. The background correction is less than 1% for all measured ions species except for O^+ which overlaps with water vapor, the principal background gas in the vacuum system. The background correction for the O^+ signal is less than 10%.

Figure 3 shows the ion arrival position distributions for both CO_2^+ and O^+. The CO_2^+ parent ions, which are formed with thermal energy, impact on a narrow strip located immediately beneath the electron beam while the energetic O^+ fragment ions are detected over a much wider area of the PSD. From the arrival position distributions, it was determined that all product ions were completely collected. Cross sections for CO_2 were initially measured using a PSD with a diameter of 25 mm. A few of the more energetic fragment ions, however, impacted near the edges of the PSD and to demonstrate that they were being completely collected, the cross sections were remeasured at selected energies using a larger PSD with a diameter of 40 mm. To within the uncertainties stated in Table I, no changes in the measured cross

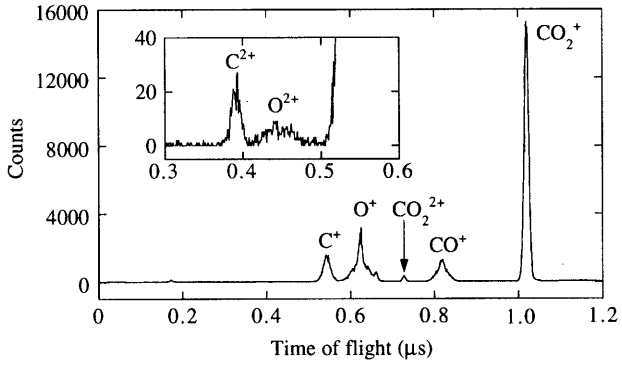

FIG. 2. Time-of-flight spectrum for ions produced by 200 eV electron impact on CO_2. The peak on the right-hand shoulder of the O^+ peak is due to water vapor, the principle background gas in the vacuum system.

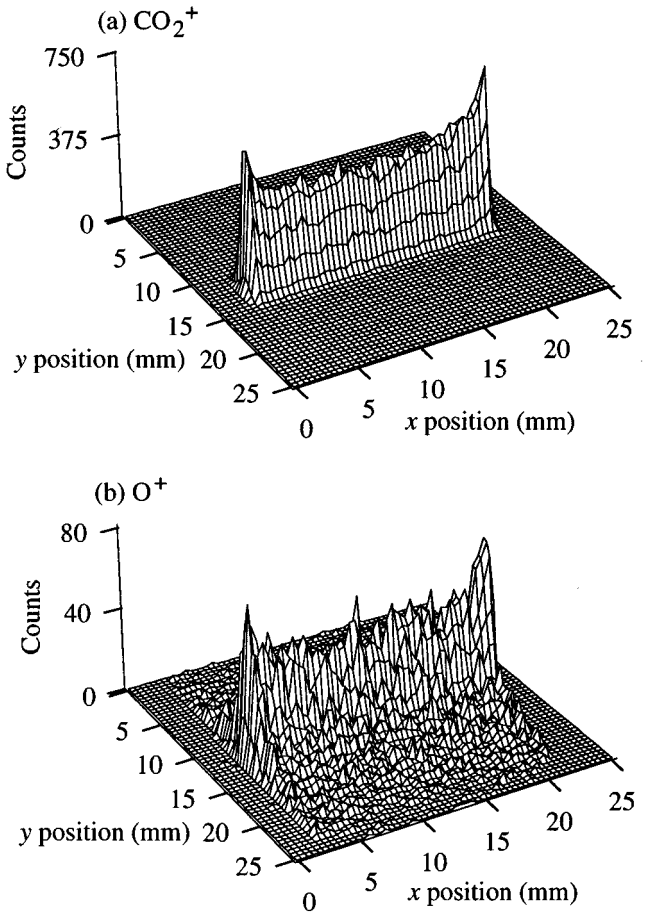

FIG. 3. Arrival position distributions for (a) CO_2^+ and (b) O^+ ions produced by 1000 eV electron impact on CO_2. The electron beam is parallel to the x direction.

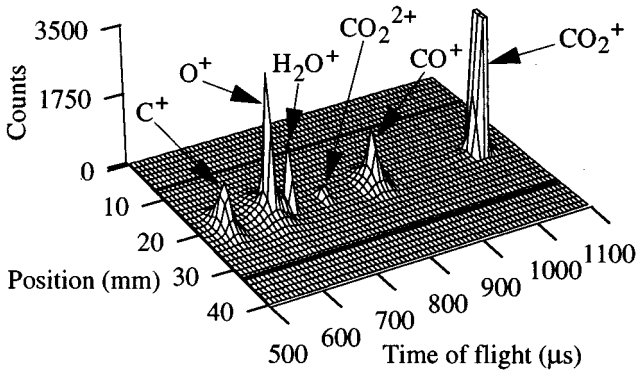

FIG. 4. Position and time-of-flight distribution produced by 1000 eV electron impact on CO_2. This distribution was obtained with a 40 mm diameter PSD and the bold lines at positions of 7.5 mm and 32.5 mm indicate the boundaries of the 25 mm diameter PSD.

sections were observed, demonstrating that all of the energetic fragment ions were indeed being collected with the 25 mm diameter PSD. From a knowledge of an ion's flight time and the geometry of the apparatus, the maximum kinetic energy of a fragment ion for which there is complete collection is readily calculated. For the 40 mm diameter PSD, CO^+ ions with kinetic energies up to 38 eV, O^+ ions with kinetic energies up to 33 eV, C^+ ions with kinetic energies up to 31 eV, O^{2+} ions with kinetic energies up to 56 eV, and C^{2+} ions with kinetic energies up to 52 eV are completely collected.

TABLE I. Ion counting statistics and the relative and absolute uncertainties associated with the partial cross sections for CO_2. The ion counting statistics represent one standard deviation. The uncertainty for σ(Total) comes from an appropriately weighted sum of the uncertainties for the partial cross sections.

Cross section	Ion counting statistics (%)	Relative uncertainty (%)	Absolute uncertainty at 200 eV (%)	Absolute uncertainty at all other energies (%)
$\sigma(CO_2^+)$	0.5	±2.0	±3.0	±3.5
$\sigma(CO^+)$	1.5	±2.5	±3.5	±4.0
$\sigma(CO_2^{2+})$	3.0	±3.5	±4.0	±5.5
$\sigma(O^+)$	1.0	±2.5	±3.5	±4.0
$\sigma(C^+)$	1.5	±2.5	±3.5	±4.0
$\sigma(O^{2+})$	7.0	±7.5	±7.5	±10.5
$\sigma(C^{2+})$	7.0	±7.5	±7.5	±10.5
σ(Total)		±2.0	±3.0	±3.5

An alternative way of presenting the data is illustrated in Fig. 4 in which the ion arrival position distributions of the type shown in Fig. 3 are integrated along the electron beam axis (the x direction in Fig. 3) and combined with the time-of-flight spectrum. The data shown in Fig. 4 were obtained with the 40 mm diameter PSD and it is evident that all ions are collected for both the 25 mm diameter and 40 mm diameter PSD's. The widths in both position and time of the singly and doubly ionized parent molecule peaks are due to the spatial extent of the electron beam while the greater widths for the fragment ion peaks are due primarily to the fragment ions' initial velocities perpendicular to the electron beam. Figure 5 shows similar plots obtained for CO_2 at three additional electron energies. These plots show that while the maximum kinetic energies of fragment ions increase with increasing electron energy there always appears to be a low energy component. Figure 6 is the same type of plot for O^{2+} and C^{2+} at an electron energy of 200 eV. Although the statistics in Fig. 6 are poor due to the small cross sections for production of O^{2+} and C^{2+} ($\sim 3\times 10^{-19}$ cm^2), a striking difference can be seen between the energy distributions of the two fragment ions. The O^{2+} energy distribution is very energetic while the C^{2+} energy distribution looks like the thermal energy distributions of the singly and doubly ionized parent molecule peaks. The most likely mechanism for the production of thermal C^{2+} is by the direct dissociation of CO_2^{2+} into C^{2+} and two neutral oxygen atoms in which the oxygen atoms carry away the excess energy.

Determination of l, the effective path length along the electron beam from which the collected ions originate, was discussed previously[15] for argon ions. It was shown that the

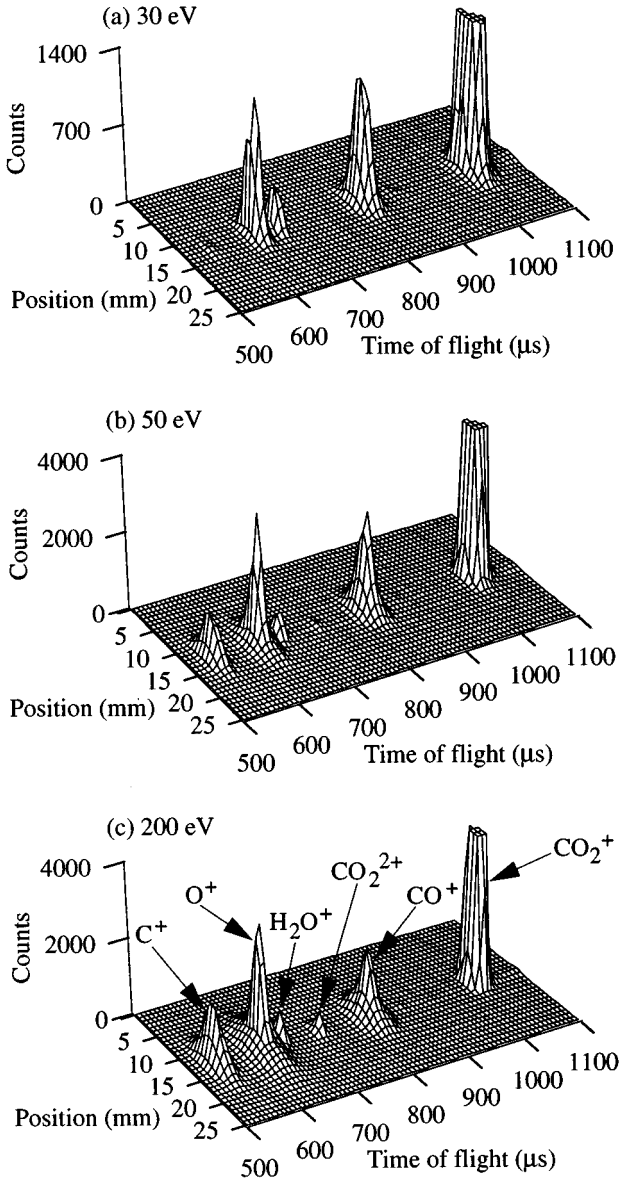

FIG. 5. Position and time-of-flight distributions produced by (a) 30 eV, (b) 50 eV, and (c) 200 eV electron impact on CO_2. These distributions were obtained with a 25 mm diameter PSD.

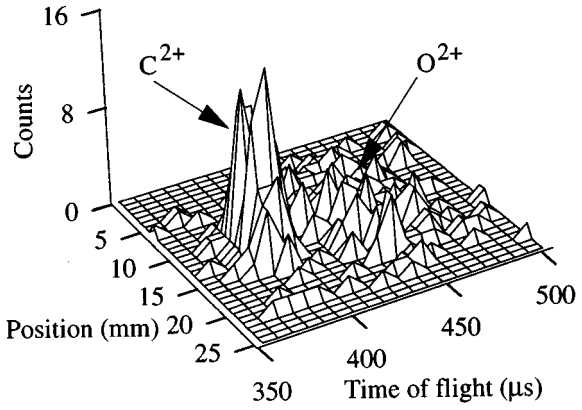

FIG. 6. Position and time-of-flight distribution for doubly charged fragment ions produced by 200 eV electron impact on CO_2. The distribution was obtained with a 25 mm diameter PSD.

high degree of uniformity of the extraction field coupled with the fact that all argon ions were formed with thermal energy ensured that ions impacting the PSD had originated from a region, directly above the aperture in the bottom plate, whose effective length was equal to the 1.91 cm length of the aperture. In the present measurements, fragment ions resulting from dissociative ionization may have energies of several electron volts and in consequence some ions created in the region directly above the aperture with velocities parallel to the electron-beam axis will escape detection. For example, a 10 eV O^+ ion having all of its initial velocity parallel to the electron-beam axis will travel 0.8 cm parallel to the electron-beam axis before reaching the bottom plate. However, the translational symmetry of the apparatus along the electron-beam axis and the uniformity of the extraction field ensures that for every ion produced in the region directly above the PSD that escapes detection, one from outside this region will be detected. In the case of 10 eV O^+, ions that impact the PSD actually come from a region that is 3.5 cm long although the effective length from which they originate is still given by the 1.91 cm length of the aperture in front of the PSD. Since the top and bottom plates are 19 cm long in the direction parallel to the electron-beam axis, all detected ions originate in a region far removed from the outer edges of the electrodes, and thus, in a region where the electric field is highly uniform.

III. CROSS SECTION MEASUREMENTS

Measurement of all the quantities on the right-hand side of Eq. (1) allows direct determination of absolute partial cross sections. Since measurements of n are extremely time consuming, absolute measurements of the cross section for single ionization of the parent molecule were made only at a limited number of electron energies. The relative shapes of the partial cross sections were determined by measuring the cross sections at various energies relative to the cross section at an electron energy of 200 eV. The absolute cross sections measured at several additional energies were compared to the relative curve normalized at 200 eV as a consistency check and found to agree. Checks were performed that established the independence of the measured cross sections with respect to variations in both the CO_2 pressure and electron beam current.

A detailed analysis of the experimental uncertainties has been given previously.[15] Table I gives the ion counting statistics and the relative and absolute uncertainties for all cross sections measured in this work. The relative uncertainties come from the ion counting statistics and a $\pm 0.5\%$ uncertainty in the electron beam current measurement. The absolute uncertainties in the cross sections come from the ion

TABLE II. Results for the partial cross sections of CO_2.

Energy (eV)	$\sigma(CO_2^+)$ (10^{-16} cm^2)	$\sigma(CO^+)$ (10^{-17} cm^2)	$\sigma(CO_2^{2+})$ (10^{-18} cm^2)	$\sigma(O^+)$ (10^{-17} cm^2)	$\sigma(C^+)$ (10^{-17} cm^2)	$\sigma(O^{2+})$ (10^{-19} cm^2)	$\sigma(C^{2+})$ (10^{-19} cm^2)
15	0.143						
20	0.564						
25	1.04	0.300		0.451			
30	1.44	1.49		1.06	0.026		
35	1.64	2.65		1.60	0.300		
40	1.82	3.01		2.09	0.837		
45	1.96	3.20	0.178	2.62	1.29		
50	2.06	3.40	0.419	3.18	1.59		
55	2.13	3.61	0.730	3.74	1.90		
60	2.19	3.85	1.13	4.32	2.21		
65	2.23	3.91	1.33	4.79	2.43		
70	2.26	4.02	1.69	5.14	2.61		
75	2.28	4.02	1.82	5.57	2.76		
80	2.31	4.08	2.18	5.89	2.94		0.189
85	2.33	4.11	2.31	6.17	3.01		0.227
90	2.35	4.12	2.39	6.40	3.13		0.328
95	2.36	4.11	2.60	6.57	3.23	0.179	0.534
100	2.37	4.10	2.80	6.75	3.27	0.208	0.548
110	2.35	4.06	2.99	6.98	3.39	0.342	0.791
120	2.34	3.98	3.04	7.06	3.39	0.757	1.13
140	2.30	3.83	3.09	7.13	3.47	1.39	1.65
160	2.22	3.56	3.03	7.01	3.36	1.67	1.95
180	2.17	3.48	2.97	6.75	3.23	2.26	2.60
200	2.10	3.27	2.84	6.58	3.13	2.43	2.91
225	2.03	3.12	2.68	6.31	3.00	2.82	2.67
250	1.95	2.88	2.41	5.94	2.83	2.97	3.02
275	1.90	2.79	2.39	5.73	2.70	3.15	2.56
300	1.81	2.59	2.10	5.43	2.54	2.86	2.61
350	1.67	2.34	1.90	4.86	2.23	2.57	2.23
400	1.59	2.17	1.80	4.47	2.08	2.21	2.31
450	1.47	1.99	1.70	3.99	1.88	1.98	2.04
500	1.38	1.83	1.45	3.71	1.73	1.97	1.82
550	1.30	1.70	1.31	3.47	1.58	1.73	1.89
600	1.24	1.58	1.28	3.19	1.49	1.59	1.48
650	1.18	1.48	1.15	3.06	1.39	1.45	1.73
700	1.13	1.42	1.08	2.89	1.30	1.79	1.50
750	1.08	1.34	1.01	2.73	1.25	1.50	1.60
800	1.03	1.26	0.979	2.57	1.18	1.29	1.41
850	0.981	1.21	0.900	2.43	1.10	1.29	1.31
900	0.957	1.15	0.837	2.33	1.06	1.02	0.982
950	0.924	1.11	0.753	2.26	1.02	1.17	0.912
1000	0.890	1.05	0.735	2.12	0.979	1.04	1.00

counting statistics, a $\pm 0.5\%$ uncertainty associated with determination of the detection efficiency, a $\pm 0.5\%$ uncertainty in the electron beam current measurement, a $\pm 0.5\%$ uncertainty in the calibration of the electrometer used for the electron beam current measurement and PSD detection efficiency determination, a $\pm 1\%$ uncertainty in the target length, a $\pm 2.5\%$ statistical uncertainty and a $\pm 1\%$ calibration uncertainty in the pressure measurement with the capacitance diaphragm gauge, and a $\pm 0.2\%$ uncertainty in the temperature measurement needed for calculation of the number density. The energy of the electron beam was established to better than ± 1 eV by observing the threshold for He^+ formation.

IV. RESULTS AND DISCUSSION

The measured partial cross sections for CO_2 are listed in Table II and are plotted in Figs. 7–11 together with previously published partial cross sections. The total cross section is shown in Fig. 12 together with previously published direct measurements of the total cross section. The total cross section shown is the sum of the partial cross sections weighted by the charge of the ion (i.e., the gross ionization cross section). The total cross section of Rapp and Englander-Golden[5] agrees well with the present measurements to within the combined uncertainties. The results of Asundi, Kurepa, and Craggs[6] lie higher than the present results probably due to their measurement of the CO_2 pressure using a McLeod gauge uncorrected for the mercury pumping effect.

Of all the partial cross sections shown in Figs. 7–11, only the present results and those of Freund, Wetzel, and Shul[8] are absolute. All of the remaining partial cross sections were ultimately normalized to either a rare gas or CO_2 absolute total cross section measured by Rapp and

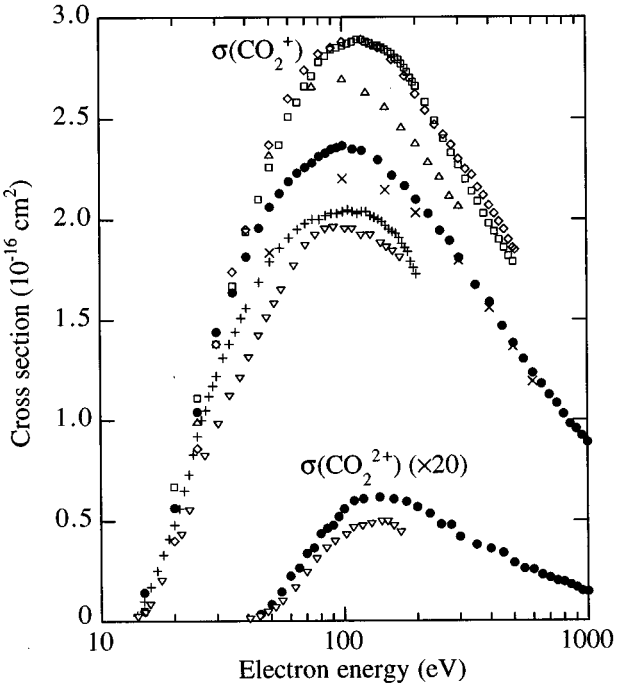

FIG. 7. Present CO_2^+ and CO_2^{2+} cross sections (●) together with the results of Freund, Wetzel, and Shul (Ref. 8) (+); Orient and Srivastava (Ref. 9) (◇); Märk and Hille (Ref. 10) (▽); Crowe and McConkey (Ref. 11) (△); Adamczyk, Boerboom, and Lukasiewicz (Ref. 12) (×); and Krishnakumar (Ref. 13) (□).

Englander-Golden[5] except for the results of Orient and Srivastava[9] which were normalized using the rare gas cross sections recommended by Märk[17] which agree very well with the rare gas cross sections of Rapp and Englander-Golden.[5] Since the present CO_2 measurement and previous Ar measurement[15] agree well with the results of Rapp and Englander-Golden, comparison between the present results and previous partial cross section measurements which were normalized to Rapp and Englander-Golden's results should be meaningful; however, if thermal-energy parent ions are collected with a higher efficiency than energetic fragment ions, normalizing to a total cross section of Rapp and Englander-Golden would result in parent ion cross sections being too high and the corresponding fragment ion cross sections being too low.

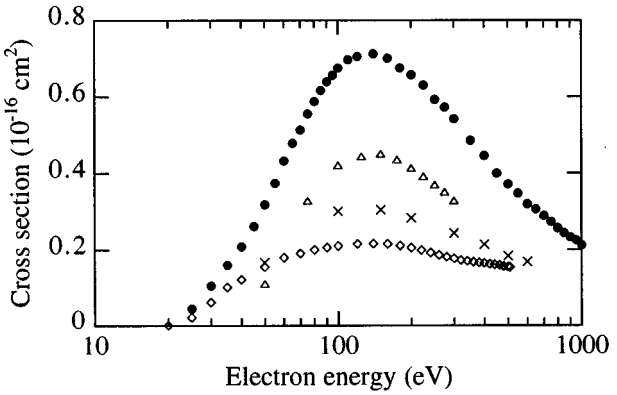

FIG. 9. Present O^+ cross section (●) together with the results of Orient and Srivastava (Ref. 9) (◇); Crowe and McConkey (Ref. 11) (△); and Adamczyk, Boerboom, and Lukasiewicz (Ref. 12) (×).

For the CO_2^+ cross section, there is a very large spread in the measured values, however, the results of Freund, Wetzel, and Shul;[8] Orient and Srivastava;[9] Crowe and McConkey;[11] Adamczyk, Boerboom, and Lukasiewicz;[12] and Krishnakumar[13] each agree with the present result to within the combined uncertainties. It should be noted, that previous measurements generally report uncertainties of $\pm 10\%$ to $\pm 15\%$ while the uncertainty for the present CO_2^+ cross section is $\pm 3.5\%$. For both CO_2^+ and CO_2^{2+}, the results of Märk and Hille[10] fall lower than the present results and do not agree to within the combined uncertainties. For CO_2^{2+}, it should be mentioned that Newton and Sciamanna[18] reported that at an electron energy of 80 eV approximately 30% of the CO_2^{2+} is formed in a metastable state that dissociates into CO^+ and

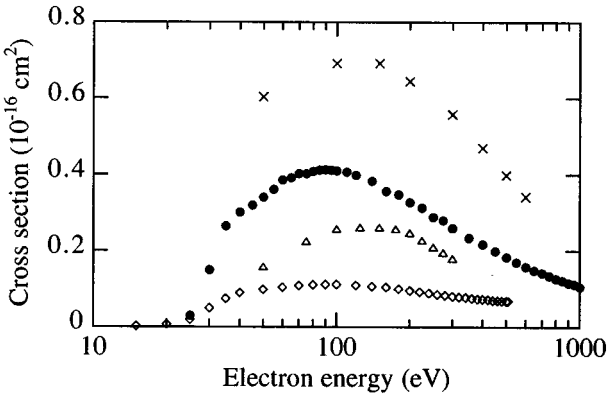

FIG. 8. Present CO^+ cross section (●) together with the results of Orient and Srivastava (Ref. 9) (◇); Crowe and McConkey (Ref. 11) (△); and Adamczyk, Boerboom, and Lukasiewicz (Ref. 12) (×).

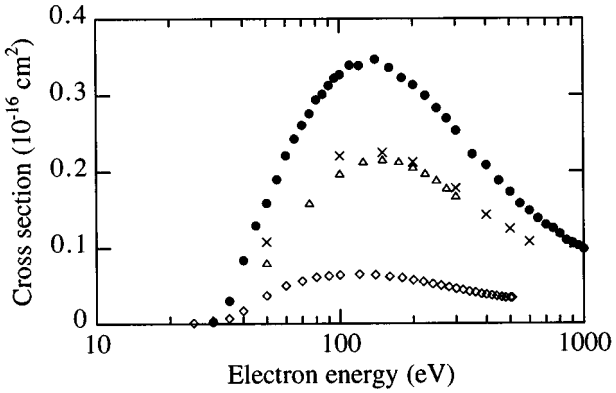

FIG. 10. Present C^+ cross section (●) together with the results of Orient and Srivastava (Ref. 9) (◇); Crowe and McConkey (Ref. 11) (△); and Adamczyk, Boerboom, and Lukasiewicz (Ref. 12) (×).

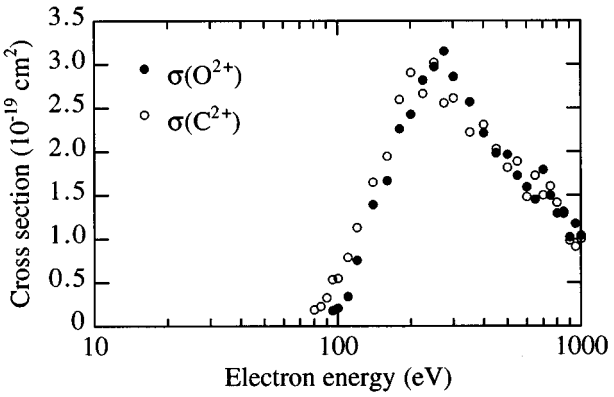

FIG. 11. Present O^{2+} and C^{2+} cross sections.

O^+ with a half-life of 2.3 μs. If this is the case, approximately 7% of the CO_2^{2+} formed in the present experiment would not have been detected. Additionally, since the CO_2^{2+} takes longer to reach the detector in Märk and Hille's experiment, part of the difference between the present CO_2^{2+} results and those of Märk and Hille could be explained by the loss of metastable CO_2^{2+}.

For the CO^+, O^+, and C^+ cross sections, the previous results show very poor agreement with those presented here and, with the exception of Adamczyk, Boerboom, and Lukasiewicz's[12] CO^+ cross section, always fall lower than the present data. None of the previous measurements agrees with the present results to within the combined uncertainties. Crowe and McConkey[11] discuss the possibility that the cross section ratios of Adamczyk, Boerboom, and Lukasiewicz[12] are in error due to an excessively high CO_2 pressure in their mass spectrometer. The results of Orient and Srivastava,[9] which are the most recent results, exhibit the poorest agreement with the present data and are lower by a factor of approximately 3 for CO^+ and O^+ and a factor of approximately 5 for C^+. The low cross sections of Orient and Srivastava and of others are probably attributable to the incomplete collection of energetic fragments. Only the present experiment conclusively demonstrates the collection of all product ions from CO_2. The results of Rapp, Englander-Golden, and Briglia,[14] who measured the cross section for production of ions with kinetic energies greater than 0.25 eV, are not shown here but their cross section values are similar to those of Crowe and McConkey.[11]

Figure 11 shows the measured cross sections for O^{2+} and C^{2+} for which there are no known previous measurements. Additionally, no evidence was seen for the production of either O_2^+ or CO^{2+} from CO_2 by electron impact. Determination of the existence of either O_2^+ or CO^{2+} is difficult due to the fact that their flight times would place them very close to the peaks of other fragment ions (next to CO^+ for O_2^+ and between O^+ and C^+ for CO^{2+}). From the data obtained with the present apparatus, the cross sections for O_2^+ and CO^{2+} are estimated to be less than 10^{-19} and 10^{-18} cm^2, respectively, at an electron energy of 200 eV.

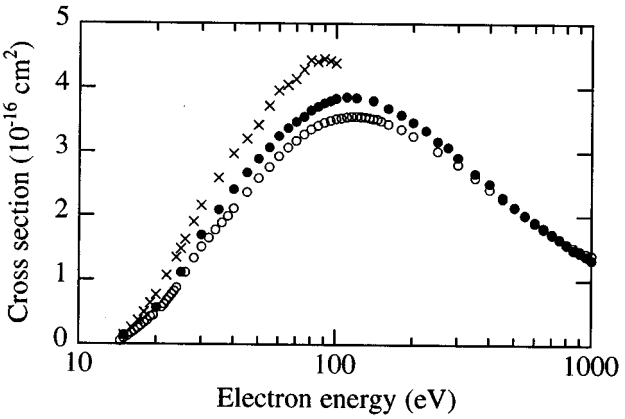

FIG. 12. Present CO_2 total cross section (●) together with the results of Rapp and Englander-Golden (Ref. 5) (○) and Asundi, Craggs, and Kurepa (Ref. 6) (×).

V. CONCLUSION

Measurements of the absolute partial cross section for electron-impact ionization of CO_2 have been presented. The apparatus geometry is of simple design embodying a short-path-length time-of-flight mass spectrometer and position-sensitive detection of the product ions, and thus, allows the complete collection of energetic fragment ions, from dissociative ionization to be unequivocally demonstrated. Additionally, determination of the ions' detection efficiency and direct measurement of the CO_2 gas pressure using a capacitance diaphragm gauge allows cross sections to be measured absolutely. The present cross section measurements have been compared to previous results. Particularly, previous measurements for energetic fragment ion cross sections disagree with the present results and are generally observed to be lower than the present data.

ACKNOWLEDGMENTS

We gratefully acknowledge support by the Atmospheric Sciences Section of the National Science Foundation, the National Aeronautics and Space Administration, and the Robert A. Welch Foundation.

[1] L. J. Kieffer and G. H. Dunn, Rev. Mod. Phys. **38**, 1 (1966).
[2] T. D. Märk, Beitr. Plasmaphys. **22**, 257 (1982).
[3] *Electron Impact Ionization*, edited by T. D. Märk and G. H. Dunn (Springer, New York, 1985).
[4] M. A. Lennon, K. L. Bell, H. B. Gilbody, J. G. Hughes, A. E. Kingston, M. J. Murray, and F. J. Smith, J. Phys. Chem. Ref. Data **17**, 1285 (1988).
[5] D. Rapp and P. Englander-Golden, J. Chem. Phys. **43**, 1464 (1965).
[6] R. K. Asundi, J. D. Craggs, and M. V. Kurepa, Proc. Phys. Soc. **82**, 967 (1963).
[7] P. T. Smith, Phys. Rev. **36**, 1293 (1930); J. T. Tate and P. T. Smith, *ibid.* **39**, 270 (1932).
[8] R. S. Freund, R. C. Wetzel, and R. J. Shul, Phys. Rev. A **41**, 5861 (1990).
[9] O. J. Orient and S. K. Srivastava, J. Phys. B **20**, 3923 (1987).
[10] T. D. Märk and E. Hille, J. Chem. Phys. **69**, 2492 (1978).
[11] A. Crowe and J. W. McConkey, J. Phys. B **7**, 349 (1974).

[12] B. Adamczyk, A. J. H. Boerboom, and M. Lukasiewicz, Int. J. Mass Spectrom. Ion Phys. **9**, 407 (1972).
[13] E. Krishnakumar, Int. J. Mass Spectrom. Ion Proc. **97**, 283 (1990).
[14] D. Rapp, P. Englander-Golden, and D. D. Briglia, J. Chem. Phys. **42**, 4081 (1965).
[15] H. C. Straub, P. Renault, B. G. Lindsay, K. A. Smith, and R. F. Stebbings, Phys. Rev. A **52**, 1115 (1995).
[16] R. S. Gao, P. S. Gibner, J. H. Newman, K. A. Smith, and R. F. Stebbings, Rev. Sci. Instrum. **55**, 1756 (1984).
[17] T. D. Märk, in *Electron Impact Ionization*, edited by T. D. Märk and G. H. Dunn (Springer, New York, 1985), p. 137.
[18] A. S. Newton and A. F. Sciamanna, J. Chem. Phys. **40**, 718 (1964).